Earth Syst. Dynam., 8, 865–873, 2017
https://doi.org/10.5194/esd-8-865-2017

Earth System Dynamics
Open Access
EGU

Climatology of Lyapunov exponents: the link between atmospheric rivers and large-scale mixing variability

Daniel Garaboa-Paz, Jorge Eiras-Barca, and Vicente Pérez-Muñuzuri

Group of Nonlinear Physics, Faculty of Physics, University of Santiago de Compostela, 15782 Santiago de Compostela, Spain

Correspondence to: Vicente Pérez-Muñuzuri (vicente.perez@cesga.es)
and Daniel Garaboa-Paz (angeldaniel.garaboa@usc.es)

Received: 2 January 2017 – Discussion started: 26 January 2017
Revised: 31 July 2017 – Accepted: 11 August 2017 – Published: 26 September 2017

Abstract. Large-scale tropospheric mixing and Lagrangian transport properties have been analyzed for the long-term period 1979–2014 in terms of the finite-time Lyapunov exponents (FTLEs). Wind field reanalyses from the European Centre for Medium-Range Weather Forecasts were used to calculate the Lagrangian trajectories of large ensembles of particles. Larger values of the interannual and intra-annual mixing variabilities highlight the El Niño Southern Oscillation, the storm track, or the Intertropical Convergence Zone among other large-scale structures. The mean baroclinic instability growth rate and the mean atmospheric river occurrence show large correlation values with the FTLE climatology as an indication of their influence on tropospheric mixing in the midlatitudes. As a case study, the role that land-falling atmospheric rivers have on large-scale tropospheric mixing and the precipitation rates observed in Saharan Morocco and the British Isles has been analyzed. The atmospheric river contribution to tropospheric mixing is found to decrease from 15 % in Saharan Morocco to less than 5 % for the UK and Ireland regions, in agreement with their contribution to precipitation that is 40 % larger in the former than in the latter region.

1 Introduction

Large-scale tropospheric mixing and transport barriers to air masses play an important role in characterizing weather. Together with the Coriolis effect and the distribution of the continents, the conversion of thermal into kinetic energy is the main triggering mechanism regulating large-scale atmospheric circulation. Extratropical cyclones and jets outside of the tropics, monsoons, and hurricanes in the tropics, among others, are the main structures for tropospheric mixing.

Many efforts have been devoted to studying the state of the atmosphere in terms of spatial distributions and the intensity of the mentioned structures based on GCMs (global circulation models) and reanalysis data to analyze current and future climate scenarios. The identification of storms tracks (Bengtsson et al., 2006), tropical and extratropical cyclones (Bengtsson et al., 2007; Ulbrich et al., 2009; Lehmann et al., 2014), jets in the middle latitudes (Barnes and Polvani, 2013), and their activity associated with modes of climate variability show that changes in the atmospheric circulation are important, affecting the transport of energy, momentum, water vapor, and thus the mixing processes present in the atmosphere.

In particular, tropospheric or atmospheric rivers (ARs) have been shown to play a key role in extratropical tropospheric dynamics (Newel et al., 1994; Zhu and Newell, 1998; Gimeno et al., 2016). These structures are narrow and elongated filaments that transport moisture from the tropics into the midlatitudes over a period of a few days once a baroclinic structure develops. For some AR events, a filament pattern develops and lasts long enough to be considered a Lagrangian coherent structure (Garaboa-Paz et al., 2015). The advection and convergence of moisture by ARs is a key process for the Earth's sensible and latent heat redistribution and has a strong impact on the water cycle of the midlatitudes, increasing tropospheric mixing. Additionally, the importance of a better understanding of ARs is undoubtedly key, since

they have been shown to be closely related to extreme precipitation and flooding events in different parts of the world (Dettinger et al., 2011; Ralph et al., 2011; Lavers et al., 2013; Eiras-Barca et al., 2016).

Considering that all sources of large-scale tropospheric mixing necessary for a detailed mixing climatology would be overwhelming, it is necessary to find new variables or proxies to measure the current climate state and the main variability sources in terms of mixing. Lehmann et al. (2014) have reported the link between large-scale baroclinicity represented by the maximum Eady growth rate and the storm track. Baroclinicity is one of the main mechanisms that addresses the transport of air masses within the troposphere in the midlatitudes (Lindzen and Farrell, 1980; Hoskins and Valdes, 1990). These regions are dominated by cyclone and anticyclone activity that increase tropospheric mixing, in contrast to tropical and subtropical latitudes.

Anther approach to characterizing mixing and transport is by calculating the Lagrangian trajectories of passive tracers in the atmosphere. The link between transport and climate, in terms of long-term statistics of Lagrangian quantities (James, 2003; Stohl, 2006), and the global climate change variability in tropospheric mixing (Holzer and Boer, 2001) has been previously studied. Among the different statistics that can be calculated (dispersion, diffusivity, etc), finite-time Lyapunov exponents (FTLEs) measure the separation rate of two trajectories over time from initially nearby starting points, i.e., the local stretching rates at a finite time. FTLEs have been used to identify the presence of barriers to mixing in the atmosphere between the tropics and extratropics (Pierrehumbert and Yang, 1993) and to study the zonal stratospheric jet (Beron-Vera et al., 2008), jet streams (Tang et al., 2010), hurricanes (Rutherford et al., 2012), transient baroclinic eddies (von Hardenberg and Lunkeit, 2002), and the polar vortex (Koh and Legras, 2002). The predictability of the atmosphere for long periods of time has also been studied using FTLEs (Yoden and Nomura, 1993; Huber et al., 2001; Stohl, 2001; Garny et al., 2007; d'Ovidio et al., 2009; Ding et al., 2015; Garaboa-Paz et al., 2017). Moreover, the identification of ridges of maximum FTLEs (Shadden et al., 2005) allows for the detection of potential Lagrangian coherent structures or kinematic transport barriers that control flow mixing and folding over a period of time for the examples cited above.

Here, two scientific objectives are addressed: first, we study the large-scale mixing variability in the lower troposphere at synoptic timescales for the current climate period. Second, we study the role played by different sources of mixing. Thus, we analyze the effect of baroclinic instabilities and Eady growth rate as well as the effect that the advective moisture transport from the (sub)tropics led by ARs has on tropospheric mixing.

To address the first objective, we investigate the long-term variability in tropospheric mixing using the FTLE and focusing on the role that large-scale structures with a timescale of days play in global horizontal transport in the lower troposphere. To that end, we have calculated a climatology of FTLEs for the period 1979–2014 using wind fields retrieved from the European Centre for Medium-Range Weather Forecast (ECMWF) reanalysis, ERA-Interim (Dee et al., 2011). Intra-annual and interannual changes in the FTLE time series over this long-term period have been studied. We show that the mean FTLE and its variability reveal inhomogeneities in mixing determined by regions of strong or weak mixing and barriers to air exchange.

For the second objective, baroclinic instability regions and the occurrence of atmospheric rivers have been calculated for the same period as the FTLEs, showing a large correlation between the two global patterns, mostly for the midlatitudes. A case study over the Atlantic region has been carried out to analyze mixing effects at smaller scales. Particularly, the contribution of land-falling ARs to tropospheric mixing was found to decrease from 15 % in Saharan Morocco to 5 % for the British Isles, in agreement with a larger contribution to precipitation in the southern region.

2 Data and methods

Atmospheric transport has been studied using wind field data retrieved from the European Centre for Medium-Range Weather Forecast reanalysis, ERA-Interim (Dee et al., 2011), with a horizontal spatial resolution of 0.7°, a vertical resolution of 100 hPa, and a temporal resolution of 6 h.

In a longitude–latitude–pressure coordinate system (ϕ, θ, P), the position of an air particle $\boldsymbol{r}(t) = (\phi(t), \theta(t), P(t))$ is calculated as $\dot{\boldsymbol{r}}(t) = \boldsymbol{v}(\boldsymbol{r}(t), t)$ and

$$\begin{aligned} \dot{\phi}(t) &= \frac{u(\boldsymbol{r}(t), t)}{R\cos(\theta(t))} \\ \dot{\theta}(t) &= \frac{v(\boldsymbol{r}(t), t)}{R} \\ \dot{P}(t) &= w(\boldsymbol{r}(t), t), \end{aligned} \tag{1}$$

where u, v, and w are the eastward, northward, and vertical wind components, respectively, and $R \approx 6370$ km is the Earth's mean radius.

A fine grid of particles with an initial separation of 0.35° is uniformly distributed on the 850 hPa level to avoid the interference of most of the turbulence effects from the boundary layer covering the domain $\boldsymbol{r}(t_0) = \{(\theta_0, \phi_0) \in [0, 360] \times [-85, 85]\}$ at time instant t_0. Then, 3-D Lagrangian simulations have been performed so that particle trajectories $\boldsymbol{r}(t; t_0, \boldsymbol{r_0})$ are computed integrating Eq. (1) using a fourth-order Runge–Kutta scheme with a fixed time step of $\Delta t =$ 1.5 h and multilinear interpolation in time and space.

In order to characterize the atmospheric transport, we introduce the finite-time Lyapunov exponents (FTLEs) that measure, at a given location, the maximum stretching rate of an infinitesimal fluid parcel over the time interval $[t_0, t_0 + \tau]$ starting at $\boldsymbol{r}(t_0; t_0, r_0) = \boldsymbol{r_0}$ and ending at $\boldsymbol{r}(t_0 + \tau; t_0, \boldsymbol{r_0})$

(Shadden et al., 2005; Sadlo and Peikert, 2007). The integration time τ must be predefined and it has to be long enough to allow trajectories to explore the coherent structures present in the flow. The FTLE fields λ are computed along the trajectories of Lagrangian tracers in the flow as (Peacock and Dabiri, 2010)

$$\lambda(\tau, t_0, \boldsymbol{r}_0) = \frac{1}{|\tau|} \log \sqrt{\mu_{\max}(\widetilde{\mathbf{C}}(\tau, t_0, \boldsymbol{r}_0))}, \quad (2)$$

where $\mu_{\max}$ is the maximum eigenvalue of the pull-back Cauchy–Green deformation tensor

$$\widetilde{\mathbf{C}}(\tau, t_0, \boldsymbol{r}_0) = (\nabla \boldsymbol{r}(t_0+\tau; t_0, \boldsymbol{r_0}))^{\mathrm{T}} \times \mathbf{G}(\theta(\tau)) \times \nabla \boldsymbol{r}(t_0+\tau; t_0, \boldsymbol{r_0}) \quad (3)$$

over a sphere (Haller and Beron-Vera, 2012), which does not take into account the deformation due to vertical movement, and $\mathbf{G}$ is the metric tensor for spherical coordinates. Repelling (attracting) coherent structures for $\tau > 0$ ($\tau < 0$) can be thought of as finite-time generalizations of the stable (unstable) manifolds of the system. These structures govern the stretching and folding mechanism that control flow mixing. Ridges in the FTLE field are used to estimate finite-time invariant manifolds in the flow that separate dynamically different regions and organize air mass transport. A positive time direction (forward FTLE) integration leads to the identification of lines of maximal divergence of air masses. In contrast, a negative time direction integration leads to the identification of areas of maximal confluence (backward FTLE). Thus, the FTLEs may be considered as a measure of the efficiency of mixing (Ottino, 1989).

The time series of the FTLE field has been computed by following the same steps explained previously but varying the initial time t_0 in fixed steps $\Delta t_0 = 6$ h in order to release a new initial tracer grid. Each FTLE field obtained for each advection from $[t_0, t_0+\tau]$ is an element of the time series $\lambda_i = \lambda(\tau, t_0 + i\,\Delta t_0, \boldsymbol{r_0})$. FTLEs are computed in the forward ($\tau > 0$) and backward ($\tau < 0$) time direction, so two time series have been generated. The finite integration times were chosen within the range $\tau \in [1, 15]$.

3 Results

We have studied the transport of air masses in terms of their FTLEs from a climatological point of view. Figure 1a shows the backward FTLEs for a given time at 850 hPa over the ocean. The structures reflect the large-scale advection of air masses, which are stretched and folded as wind transports them. The presence of ridges correspond to attracting manifolds where fluid tends to converge. Time-averaged FTLE maps for the 1979–2014 period are shown in Fig. 1b and c for forward and backward integration times, respectively. As expected in both cases, three latitudinal bands can be clearly identified in coincidence with the large-scale atmospheric

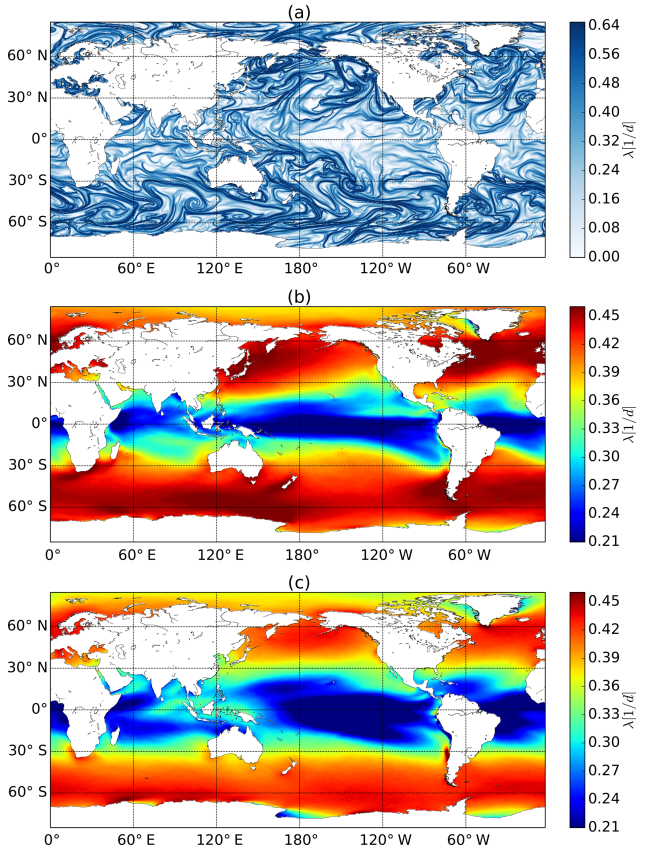

Figure 1. Backward finite-time Lyapunov exponents λ for a given day **(a)**. Local maxima in the plot (darker colors) are attracting coherent structures. Mean forward **(b)** and backward **(c)** FTLE climatology for the 1989–2014 period. For all cases, $\tau = 5$ days.

circulation belts. For the midlatitudes, FTLE values are approximately twice as high as for the Equatorial zone. A clear annual cycle is observed, and in the midlatitudes mixing is generally higher in winter than in summer (Figs. S1 and S2 in the Supplement). Note that there is some longitudinal variability in the FTLE maps depending on the presence of continents and the large-scale atmospheric circulation, as will be shown below.

Focusing on the high to middle latitudes of the forward-in-time mean FTLE maps, the signal of global pressure systems can be identified. In the Northern Hemisphere we can observe two plumes with high FTLE values over the Atlantic and Pacific oceans that correspond to the storm track, leading to an increase in mixing and dispersion. The same situation arises in the Southern Hemisphere. Moreover, the large-scale subtropical centers are apparent as elongated tongues of low FTLE values extending from the Equatorial zone to the west of continents. These regions contain low FTLE values and correspond to low mixing regions.

The mean backward FTLE field shows smaller values in Fig. 1c for high latitudes than in the forward case. Thus, the width of the region with low FTLE values near the Equa-

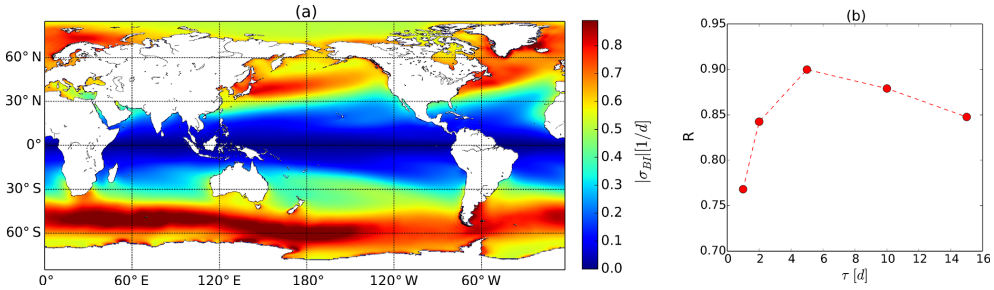

Figure 2. **(a)** Time average for 35 years of the baroclinic Eady growth rate, Eq. (4), calculated at 850 hPa. **(b)** Correlation index R between σ_{BI} and the 35-year time-averaged forward FTLE map shown in Fig. 1b for different integration times τ.

tor is larger than for the forward case. Low FTLE backward regions correspond to zones where the convergence of air masses to the Equator weakens.

Baroclinic instability is the dominant mechanism triggering the dynamics of the midlatitude weather systems. It shapes the cyclones and anticyclones that dominate weather in the midlatitudes and cause most of the large tropospheric mixing in those regions (Hartmann, 2015). The largest values of the mean FTLEs have been obtained for the midlatitudes in both hemispheres, indicating an increase in tropospheric mixing in those regions. To further quantify the connection between mixing and baroclinicity, the Eady growth rate (Lindzen and Farrell, 1980; Hoskins and Valdes, 1990) has been calculated for the 850 hPa level as

$$\sigma_{\mathrm{BI}} = 0.31 \frac{|f|}{N} \left| \frac{\partial \mathbf{V}}{\partial z} \right|, \tag{4}$$

where f is the Coriolis parameter, N is the Brunt–Väisälä frequency, $\mathbf{V}$ is the 3-D wind component, and z is the geopotential height.

Figure 2a shows the time-averaged Eady growth rate as a gridded map for the 850 hPa level for the 1979–2014 period in units of day^{-1}. Note that the storm track regions (such as the North Atlantic or North Pacific corridors) are well depicted by this measure of baroclinicity, and if compared with the mean forward-in-time FTLE map in Fig. 1b, both figures are remarkably similar. In order to quantify this coincidence, the correlation between the two fields has been calculated for different τ (Fig. 2b). A correlation maximum is observed for an integration time of 5 days, which is about the mean length of the typical synoptic timescale, in line with the mean lifetime of extratropical cyclones (e.g., Trigo, 2006). Thus, the large values of tropospheric mixing observed at the midlatitudes can be related, at least in part, to baroclinic instability.

To gain insight into the transport of air masses, the variability in the FTLE climatology has been studied in terms of the intra-annual (SD of the monthly means for the 35 years) and interannual (SD of the annual means for the 35 years) variabilities (Fig. 3). Regions where the FTLEs change between seasons correspond to a large intra-annual variability. On timescales shorter than seasonal, variability in the circulation is dominated by synoptic-scale weather systems, which prevail at that midlatitudes. The forward-in-time intra-annual variability (Fig. 3a) highlights the meridional frontier between westerly extratropical circulation and Hadley cells; larger variability is observed between seasons. As an example, note in the Pacific Ocean the plume of high variability observed that connects the semipermanent pressure system between the Aleutian Low and the North Pacific High. A similar situation can be observed between the Iceland Low and the Azores High for the Atlantic Ocean. Also note the signal of the monsoons in the Indian Ocean.

The intra-annual variability map obtained from the FTLE backward time series (Fig. 3b) shows regions with maximum variability through the year in the tropics. The main global mechanism that addresses this variability is the meridional movement of the Intertropical Convergence Zone (ITCZ). Note the importance of this variability on the African coast or in the western Pacific Ocean. The interface between the summer and winter ITCZ coincides with a region close to the Equator with small variability.

Figure 3c and d show the interannual variability calculated forward and backward in time, respectively. The interannual variability takes into account the variation through the 35 years of FTLEs computed. In this case, both forward and backward fields behave in a similar way although some differences are observed. All periodic effects are canceled out, and the El Niño Southern Oscillation (ENSO) pattern in the Pacific Ocean is shown in the backward map. Although easterly trade winds converging across the Equatorial Pacific weaken during the El Niño phase, during La Niña and neutral conditions those winds are reinforced, and the interannual backward FTLE values should be larger in the warm pool region (western Pacific) (d). However, for the forward case (c), the injection of Lagrangian particles into the Equator zone propagates with the converging trade winds and few dispersion areas within the tropics are observed. For the analyzed climate period, the variability introduced by this region is approximately 10 % of the global mean FTLE.

Comparing the interannual and intra-annual scales, the values of the intra-annual scale are clearly higher than the interannual variability in the extratropical zone; however, this

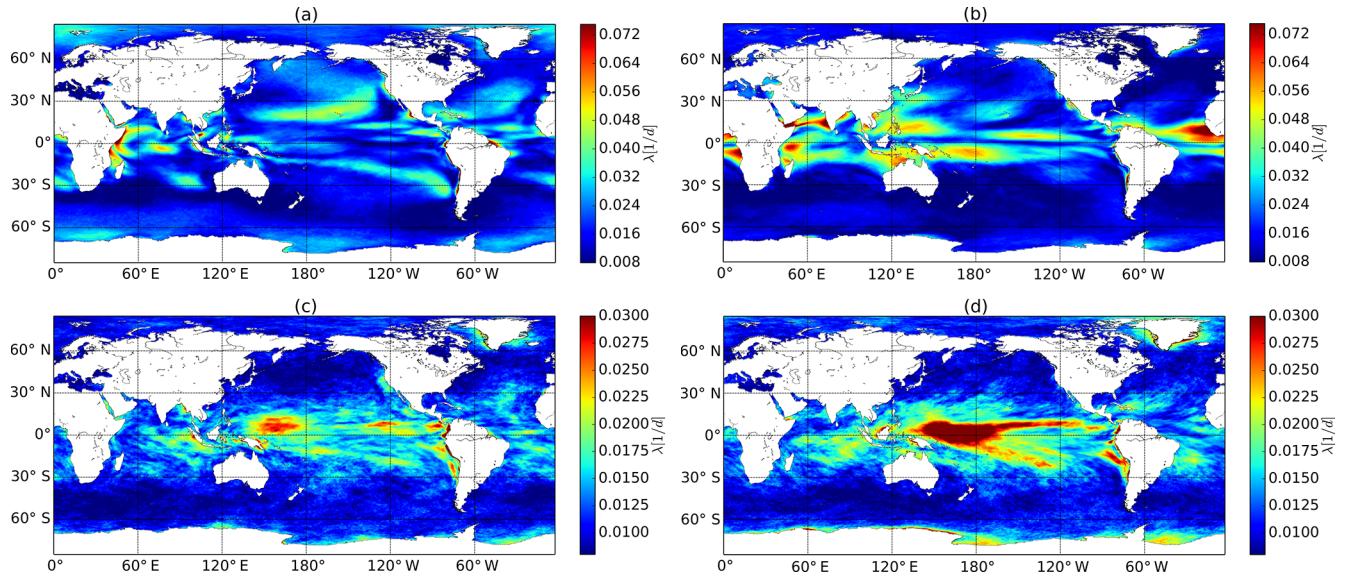

Figure 3. Seasonal dependence of the finite-time Lyapunov exponents calculated for the 1979–2014 period. Intra-annual variability in the forward **(a)** and backward **(b)** FTLE, respectively. Interannual variability in the forward **(c)** and backward **(d)** FTLE, respectively. For all cases, $\tau = 5$ days.

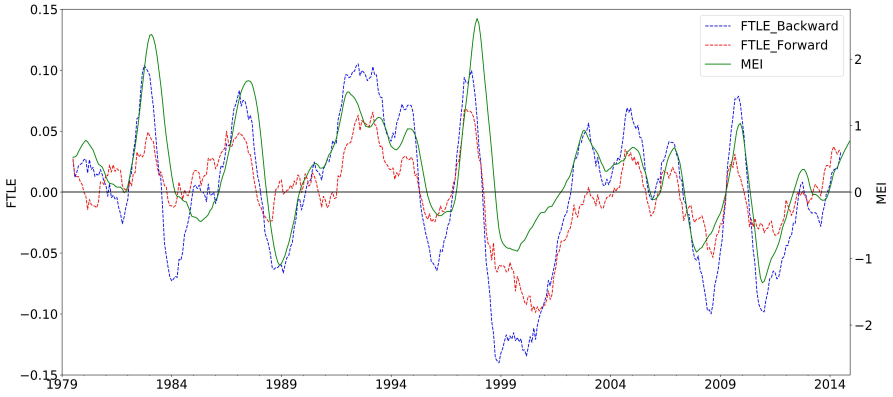

Figure 4. Monthly time evolution of the backward and forward FTLE anomalies and the MEI for the 1979–2014 period.

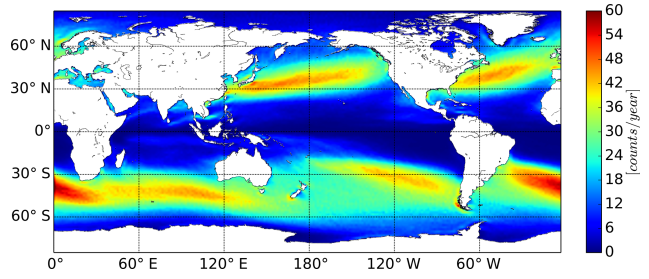

Figure 5. Mean number of atmospheric rivers detected per year. Data were retrieved from Guan and Waliser (2015) for the period 1979–2014 with a 6 h time step.

Table 1. Percentage of AR days and the associated precipitation rates out of the total for two Atlantic regions.

	Saharan Morocco	British Isles
AR days	10.3 % (1201 days)	32.5 % (3800 days)
Precipitation	16.8 %	37.5 %

difference is reduced in the Equator zone except for some zones of the western Pacific due to the ENSO.

Figure 4 elaborates on the connection between ENSO events and FTLE variability. Monthly backward and forward FTLE anomalies have been correlated with the Multivariate ENSO Index (MEI; https://www.esrl.noaa.gov/psd/enso/mei/index.html) for the western warm pool region between

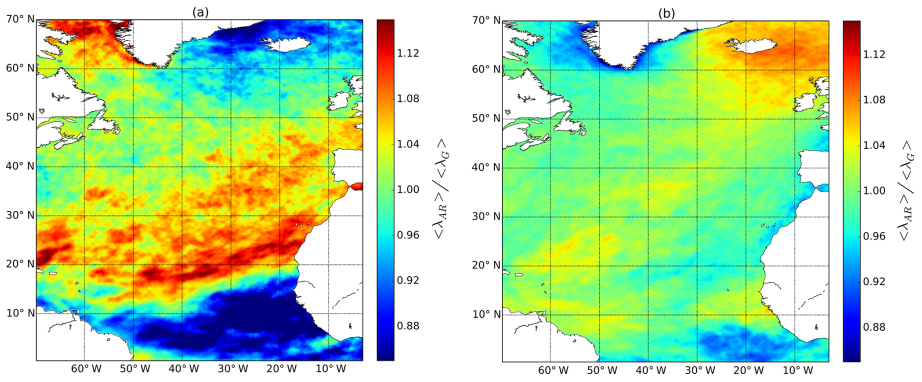

Figure 6. Ratio of the FTLE backward time series consisting of periods with land-falling atmospheric rivers and the global backward FTLE mean (Fig. 1c) for Saharan Morocco **(a)** and the UK and Ireland **(b)** regions.

140° E and 140° W and between 25° S and 25° N for the 35 years. To analyze the interannual variability in both series, we used a moving average to remove fluctuations with periods smaller than 1 year. Negative values of the MEI represent the cold ENSO phase, i.e., La Niña, while positive MEI values represent the warm ENSO phase (El Niño). Positive FTLE anomalies correlate with the El Niño phase, indicating larger FTLE values and an increase in tropospheric mixing in the studied region. On the other hand, negative FTLE anomalies correspond to small FTLE values, not favoring mixing above the sea surface. Note that backward FTLE anomalies correlate better than the forward ones in agreement with the interannual variability patterns described above (Fig. 3c and d). The obtained correlation coefficients were 0.80 and 0.64, respectively. For the Southern Oscillation Index (SOI), as expected, anticorrelated behavior with the FTLE anomaly was observed (Fig. S3).

Another important source of large-scale mixing in the atmosphere are the atmospheric rivers (ARs) that play a key role in baroclinic dynamics. ARs appear in the midlatitudes as coherent filaments of water vapor triggering tropospheric mixing and the convergence of moisture in the lower levels of the troposphere with a persistence time of several days up to 1 week (Garaboa-Paz et al., 2015). Most of the water vapor is transported from the tropics to the midlatitudes by four to five persistent ARs per hemisphere. When the atmospheric rivers make landfall, they often release this water vapor in the form of rain. To characterize their role in tropospheric mixing, the database provided by Guan and Waliser (2015) has been used to identify the presence of ARs. This database identifies ARs by complex considerations on the continuity and coherence of the integrated water vapor column and water vapor flux. Since it is able to identify ARs throughout the year and worldwide, this database is, to the best of our knowledge, the most complete AR database published (Waliser and Guan, 2017). Figure 5 shows the mean AR detections per year for the entire globe throughout the period 1979–2014. As expected, the figure identifies the main storm tracks worldwide. Such a field shows high correlation ratios with the mean baroclinic index (Fig. 2a) and the global FTLE forward mean (Fig. 1b) with values of 0.78 and 0.75, respectively. This supports the key role played by ARs in the large-scale mixing of the low troposphere. As a case study, we have focused on the contribution of ARs to tropospheric mixing and precipitation rates along the 1979–2014 period for two Atlantic regions: Saharan Morocco and the British Isles. To that end, a presence–absence time series based on AR landfall conditions over these two regions was obtained and the FTLE backward time series was filtered to isolate the AR activity.

Figure 6 shows the FTLE backward time average computed only for ARs with a positive landfall condition divided by the mean backward FTLEs over Saharan Morocco (a) and the British Isles (b). This quantity leads to the identification of regions where the AR activity has a major role in the climate background in terms of backward FTLEs. Since the FTLE ratio signal is clearly stronger for the African case, ARs should play a more prominent role in the large-scale mixing and convergence of moisture on the Saharan coast than on the British one. Therefore, this idea should be consistently kept in mind when precipitation is taken into account. Table 1 shows the rainfall during AR events out of the total in each of the two regions (see also Fig. S4). Even when AR detections are more frequent in the British Isles (32.5 % of the days) than in Saharan Morocco (10.3 % of the days), the contribution of ARs to precipitation in Saharan Morocco is 41.7 % larger than for the British Isles. The Saharan Morocco region has less AR activity than the UK and Ireland, but the contribution to precipitation is more important, in agreement with a larger anomaly in the FTLE backward mixing ratio.

4 Conclusions

The finite-time Lyapunov exponent (FTLE) time series at the 850 hPa level has been computed over a climate period of 35 years using wind fields retrieved from ERA-Interim

reanalysis data. The FTLEs provide information on areas where dispersion (integration forward in time) or convergence (backward) is large and allows for the classification of airstreams. The statistics over these Lagrangian quantities have shown the link between the climate system and regional transport structures in terms of tropospheric mixing.

This study, one of the first to estimate the current state of the troposphere in terms of mixing for a synoptical time length of days, shows mean values and intra-annual and interannual variability in the FTLEs for a 35-year period, revealing a possible link between the modes of climate variability and the mixing processes with a scale of a few days.

Mean Lyapunov exponents show a zonal localization; large values in the midlatitudes for both hemispheres, while the lowest FTLE values were observed in the intertropics. Especially in the tropics and the Equator, mixing is strongly modulated by ENSO, while for the midlatitudes, large-scale mixing is associated with the interface between westerly extratropical circulation and Hadley cells. The meridional displacement of the ITCZ has also been well reproduced by the intra-annual backward FTLE field. Seasonal effects and ENSO are the largest effects that contribute to large-scale mixing variability over the globe. Large correlation values were obtained between the monthly backward FTLEs and the MEI/SOI indices for the western warm pool region.

To support these results, we assessed the role that baroclinic instability, atmospheric rivers (ARs), and large-scale mixing measured in terms of the FTLE play in climate mixing patterns. First, the mean FTLE field was correlated to the Eady baroclinic growth rate. It was found that the best correlation is obtained for an integration time of $\tau = 5$ days, which is in agreement with the typical synoptic timescale in the midlatitudes. For larger timescales, structures observed in the intra-annual and interannual variability fields are smeared out, while for smaller τ values those structures are not well shaped, and multiple patterns arise. This suggests that baroclinicity, among other possible causes, drives large-scale tropospheric mixing on timescales longer than a few days.

On the other hand, we have observed that the number of ARs detected worldwide highly correlates with the FTLE climatology, showing the importance of the former for tropospheric mixing. To show the potential of mixing as a regional variable, we focused on the impact of land-falling ARs on the precipitation rates in the Atlantic Ocean. The advection of moisture by ARs is a key process for the Earth's sensible and latent heat redistribution and has a strong impact on the water cycle of the midlatitudes. In a previous work we found that these structures can be well described in terms of the FTLEs (Garaboa-Paz et al., 2015). Here, we find that the impact of mixing in the Saharan Morocco region is more important than for the British Isles. Although fewer ARs and low precipitation rates are observed in Saharan Morocco compared to the UK and Ireland, rain probability during AR events and mixing is larger for the former than for the latter region.

Finally, our results suggest that tropospheric mixing, as shown in terms of large FTLE values, provides useful information to characterize the state of the atmosphere. A further analysis with a high integration time to capture longer time structures or filtering other signals coming from other structures would help to better understand the spectrum of mixing inside the atmosphere, which will be useful for the analysis of future climate scenarios in the context of climate change.

Data availability. Meteorological and climatological data sets are available online. ERA-Interim data are available via http://apps.ecmwf.int/datasets/data/interim-full-daily/levtype=pl/ (Dee et al., 2011). ENSO index data (MEI and SOI) are available via https://www.esrl.noaa.gov/psd/enso/mei/index.html (Wolter, 1993) and http://www.cpc.ncep.noaa.gov/data/indices/soi (Ropelewski and Jones, 1987), respectively. Data sets for atmospheric river detection and validation were obtained from https://ucla.app.box.com/v/ARcatalog/folder/16460297135 (Guan and Waliser, 2016) and http://hydrology.princeton.edu/data/pgf/0.25deg/daily/ (Sheffield et al., 2013).

The Supplement related to this article is available online at https://doi.org/10.5194/esd-8-865-2017-supplement.

Competing interests. The authors declare that they have no conflict of interest.

Special issue statement. This article is part of the special issue "The 8th EGU Leonardo Conference: From evaporation to precipitation: the atmospheric moisture transport". It is a result of the 8th EGU Leonardo Conference, Ourense, Spain, 25–27 October 2016.

Acknowledgements. ERA-Interim data were supported by ECMWF. This work was financially supported by Ministerio de Economía y Competitividad and Xunta de Galicia (CGL2013-45932-R, GPC2015/014) and contributions by the COST Action MP1305 and CRETUS Strategic Partnership (AGRUP2015/02). All these programs are co-funded by ERDF (EU). The computational part of this work was done in the Supercomputing Center of Galicia, CESGA. We acknowledge fruitful discussions with S. Brands and G. Míguez, helpful comments by two anonymous reviewers, and Bin Guan for kindly sharing the AR database.

Edited by: Valerio Lucarini
Reviewed by: two anonymous referees

References

Barnes, E. A. and Polvani, L.: Response of the midlatitude jets, and of their variability, to increased greenhouse gases in the CMIP5 models, J. Climate, 26, 7117–7135, https://doi.org/10.1175/JCLI-D-12-00536.1, 2013.

Bengtsson, L., Hodges, K. I., and Roeckner, E.: Storm tracks and climate change, J. Climate, 19, 3518–3543, https://doi.org/10.1175/JCLI3815.1, 2006.

Bengtsson, L., Hodges, K. I., Esch, M., Keenlyside, N., Kornblueh, L., Luo, J. J., and Yamagata, T.: How may tropical cyclones change in a warmer climate?, Tellus A, 59, 539–561, https://doi.org/10.1111/j.1600-0870.2007.00251.x, 2007.

Beron-Vera, F. J., Brown, M. G., Olascoaga, M. J., Rypina, I. I., Kocak, H., and Udovydchenkov, I. A.: Zonal jets as transport barriers in planetary atmospheres, J. Atmos. Sci., 65, 3316–3326, https://doi.org/10.1175/2008JAS2579.1, 2008.

Dee, D. P., Uppala, S. M., Simmons, A. J., Berrisford, P., Poli, P., Kobayashi, S., Andrae, U., Balmaseda, M. A., Balsamo, G., Bauer, P., Bechtold, P., Beljaars, A. C. M., van de Berg, L., Bidlot, J., Bormann, N., Delsol, C., Dragani, R., Fuentes, M., Geer, A. J., Haimberger, L., Healy, S. B., Hersbach, H., Holm, E. V., Isaksen, L., Kallberg, P., Koehler, M., Matricardi, M., McNally, A. P., Monge-Sanz, B. M., Morcrette, J. J., Park, B. K., Peubey, C., de Rosnay, P., Tavolato, C., Thepaut, J. N., and Vitart, F.: The ERA-Interim reanalysis: configuration and performance of the data assimilation system, Q. J. Roy. Meteorol. Soc., 137, 553–597, https://doi.org/10.1002/qj.828, 2011 (data available at: http://apps.ecmwf.int/datasets/data/interim-full-daily/levtype=pl/).

Dettinger, M. D., Ralph, F. M., Das, T., Neiman, P. J., and Cayan, D. R.: Atmospheric rivers, floods and the water resources of California, Water, 3, 445–478, 2011.

Ding, R., Li, J., Zheng, F., Feng, J., and Liu, D.: Estimating the limit of decadal-scale climate predictability using observational data, Clim. Dynam., 46, 1563–1580, https://doi.org/10.1007/s00382-015-2662-6, 2015.

d'Ovidio, F., Shuckburgh, E., and Legras, B.: Local mixing events in the upper troposphere and lower stratosphere. Part I: Detection with the Lyapunov diffusivity, J. Atmos. Sci., 66, 3678–3694, https://doi.org/10.1175/2009JAS2982.1, 2009.

Eiras-Barca, J., Brands, S., and Míguez-Macho, G.: Seasonal variations in North Atlantic atmospheric river activity and associations with anomalous precipitation over the Iberian Atlantic Margin, J. Geophys. Res.-Atmos., 21, 931–948, 2016.

Garaboa-Paz, D., Eiras-Barca, J., Huhn, F., and Pérez-Muñuzuri, V.: Lagrangian coherent structures along atmospheric rivers, Chaos, 25, 063105, https://doi.org/10.1063/1.4919768, 2015.

Garaboa-Paz, D., Lorenzo, M. N., and Pérez-Muñuzuri, V.: Influence of finite-time Lyapunov exponents on winter precipitation over the Iberian Peninsula, Nonlin. Process Geophys., 24, 227–235, https://doi.org/10.5194/npg-24-227-2017, 2017.

Garny, H., Bodeker, G. E., and Dameris, M.: Trends and variability in stratospheric mixing: 1979–2005, Atmos. Chem. Phys., 7, 5611–5624, https://doi.org/10.5194/acp-7-5611-2007, 2007.

Gimeno, L., Dominguez, F., Nieto, R., Trigo, R., Drumond, A., Reason, C. J. C., Taschetto, A., Ramos, A. M., Kumar, R., and Marengo, J.: Major mechanisms of atmospheric moisture transport and their role in extreme precipitation events, Annu. Rev. Env. Resour., 41, 117–141, https://doi.org/10.1146/annurev-environ-110615-085558, 2016.

Guan, B. and Waliser, D. E.: Detection of atmospheric rivers: evaluation and application of an algorithm for global studies, J. Geophys. Res.-Atmos., 120, 12514–12535, https://doi.org/10.1002/2015JD024257, 2015.

Guan, B. and Waliser, D. E: University of California, Los Ángeles, AR detection database: available at: https://ucla.app.box.com/v/ARcatalog/folder/16460297135 (last access: July 2017), 2016.

Haller, G. and Beron-Vera, F. J.: Geodesic theory of transport barriers in two-dimensional flows, Physica D, 241, 1680–1702, https://doi.org/10.1016/j.physd.2012.06.012, 2012.

Hartmann, D. L.: Global Physical Climatology, 103 (Newnes Ed.), Academic Press, San Diego, 2015.

Holzer, M. and Boer, G. J.: Simulated changes in atmospheric transport climate, J. Climate, 14, 4398–4420, https://doi.org/10.1175/1520-0442(2001)014<4398:SCIATC>2.0.CO;2, 2001.

Hoskins, B. J. and Valdes, P. J.: On the existence of storm-tracks, J. Atmos. Sci., 47, 1854–1864, https://doi.org/10.1175/1520-0469(1990)047<1854:OTEOST>2.0.CO;2, 1990.

Huber, M., McWilliams, J. C., and Ghil, M.: A climatology of turbulent dispersion in the troposphere, J. Atmos. Sci., 58, 2377–2394, https://doi.org/10.1175/1520-0469(2001)058<2377:ACOTDI>2.0.CO;2, 2001.

James, P.: A 15-year climatology of stratosphere–troposphere exchange with a Lagrangian particle dispersion model. 2. Mean climate and seasonal variability, J. Geophys. Res.-Atmos., 108, 1–16, https://doi.org/10.1029/2002JD002639, 2003.

Koh, T. Y. and Legras, B.: Hyperbolic lines and the stratospheric polar vortex, Chaos, 12, 382–394, https://doi.org/10.1063/1.1480442, 2002.

Lavers, D. A. and Villarini, G.: The nexus between atmospheric rivers and extreme precipitation across Europe, Geophys. Res. Lett., 40, 3259–3264, https://doi.org/10.1002/grl.50636, 2013.

Lehmann, J., Coumou, D., Frieler, K., Eliseev, A. V, and Levermann, A.: Future changes in extratropical storm tracks and baroclinicity under climate change, Environ. Res. Lett., 9, 84002, https://doi.org/10.1088/1748-9326/9/8/084002, 2014.

Lindzen, R. S. and Farrell, B.: A simple approximate result for the maximum growth rate of baroclinic instabilities, J. Atmos. Sci., 37, 1648–1654, https://doi.org/10.1175/1520-0469(1980)037<1648:ASARFT>2.0.CO;2, 1980.

Newell, R. E., Newell, N. E., Zhu, Y., and Scott, C.: Tropospheric rivers? A pilot study, Geophys. Res. Lett., 19, 2401–2404, https://doi.org/10.1029/92GL02916, 1992.

Ottino, J. M.: The Kinematics of Mixing: Stretching, Chaos, and Transport, University Press, Cambridge, UK, 1989.

Peacock, T. and Dabiri, J.: Introduction to focus issue: lagrangian coherent structures, Chaos, 20, 017501, https://doi.org/10.1063/1.3278173, 2010.

Pierrehumbert, R. T. and Yang, H.: Global chaotic mixing on isentropic surfaces, J. Atmos. Sci., 50, 2462–2480, https://doi.org/10.1175/1520-0469(1993)050<2462:GCMOIS>2.0.CO;2, 1993.

Ralph, F. M. and Dettinger, M. D.: Storms, floods, and the science of atmospheric rivers, EOS T. Am. Geophys. Un., 92, 265–266, 2011.

Ropelewski, C. F. and Jones, P. D.: An extension of the Tahiti-Darwin southern oscillation index, Mon. Weather Rev., 115, 2161–2165, 1987 (data available at: http://www.cpc.ncep.noaa.gov/data/indices/soi).

Rutherford, B., Dangelmayr, G., and Montgomery, M. T.: Lagrangian coherent structures in tropical cyclone intensification, Atmos. Chem. Phys., 12, 5483–5507, https://doi.org/10.5194/acp-12-5483-2012, 2012.

Sadlo, F. and Peikert, R.: Efficient visualization of Lagrangian coherent structures by filtered AMR ridge extraction, IEEE T. Vis. Comput. Gr., 13, 1456–1463, https://doi.org/10.1109/TVCG.2007.70554, 2007.

Shadden, S. C., Lekien, F., and Marsden, J. E.: Definition and properties of Langrangian coherent structures from finite-time Lyapunov exponents in two-dimensional aperiodic flows, Physica D, 212, 271–304, https://doi.org/10.1016/j.physd.2005.10.007, 2005.

Sheffield, J., Goteti, G., and Wood, E. F.: Development of a 50-year high-resolution global dataset of meteorological forcings for land surface modeling, J. Climate, 19, 3088–3111, https://doi.org/10.1175/JCLI3790.1, 2006.

Sheffield, J., Goteti, G., and Wood, E. F.: Princeton University, Hydroclimatology Group, Precipitation database, available at: http://hydrology.princeton.edu/data/pgf/0.25deg/daily/ (last access: July 2017), 2013.

Stohl, A.: A 1-year Lagrangian "climatology" of airstreams in the Northern Hemisphere troposphere and lowermost stratosphere, J. Geophys. Res.-Atmos., 106, 7263–7279, https://doi.org/10.1029/2000JD900570, 2001.

Stohl, A.: Characteristics of atmospheric transport into the Arctic troposphere, J. Geophys. Res.-Atmos., 111, 1–17, https://doi.org/10.1029/2005JD006888, 2006.

Tang, W., Mathur, M., Haller, G., Hahn, D. C., and Ruggiero, F. H.: Lagrangian coherent structures near a subtropical jet stream, J. Atmos. Sci., 67, 2307–2319, https://doi.org/10.1175/2010JAS3176.1, 2010.

Trigo, I. F.: Climatology and interannual variability of storm-tracks in the Euro-Atlantic sector: a comparison between ERA-40 and NCEP/NCAR reanalyses, Clim. Dynam., 26, 127–143, https://doi.org/10.1007/s00382-005-0065-9, 2006.

Ulbrich, U., Leckebusch, G. C., and Pinto, J. G.: Extra-tropical cyclones in the present and future climate: a review, Theor. Appl. Climatol., 96, 117–131, https://doi.org/10.1007/s00704-008-0083-8, 2009.

von Hardenberg, J. and Lunkeit, A. F.: Transient chaotic mixing during a baroclinic life cycle, Chaos, 10, 1054–1500, 2002.

Waliser, D. E. and Guan, B.: Extreme winds and precipitation during landfall of atmospheric rivers, Nat. Geosci., 10, 179–183, https://doi.org/10.1038/ngeo2894, 2017.

Wolter, K.: National Oceanic and Atmospheric Administration (NOAA), Climate Prediction Center (CPC), MEI Index, available at: https://www.esrl.noaa.gov/psd/enso/mei/index.html (last access: July 2017), 1993.

Yoden, S. and Nomura, M.: Finite-time Lyapunov stability analysis and its application to atmospheric predictability, J. Atmos. Sci., 50, 1531–1543, https://doi.org/10.1175/1520-0469(1993)050<1531:FTLSAA>2.0.CO;2, 1993.

Zhu, Y. and Newell, R.: A proposed algorithm for moisture fluxes from atmospheric rivers, Mon. Weather Rev., 126, 725–735, https://doi.org/10.1175/1520-0493(1998)126<0725:APAFMF>2.0.CO;2, 1998.